

How big is a Gabor patch, and why should we care?

R. E. Fredericksen*

McGill Vision Research, 687 Pine Avenue West (H4-14), Montreal, PQ H3A 1A1, Canada

Peter J. Bex

Center for Visual Science, University of Rochester, 274 Meliora Hall, Rochester, New York 14627

Frans A. J. Verstraten

Vision Sciences Laboratory, Harvard University, 33 Kirkland Street (Room 710), Cambridge, Massachusetts 02138

Received October 5, 1995; revised manuscript received July 3, 1996; accepted August 2, 1996

We propose a two-parameter model for the perceived size (spatial extent) of a Gaussian-windowed, drifting sinusoidal luminance pattern (a Gabor patch) based on the simple assumption that perceived size is determined by detection threshold for the sinusoidal carrier. Psychophysical measures of perceived size vary with peak contrast, Gaussian standard deviation, and carrier spatial frequency in a manner predicted by the model. At suprathreshold peak contrasts Gabor perceived size is relatively unaffected by systemic noise but varies in a manner that is consistent with the influence of local contrast gain control. However, at and near threshold, systemic noise plays a major role in determining perceived size. The data and the model indicate that measures of contrast threshold using Gaussian-windowed stimuli (or any other nonflat contrast window) are determined not just by contrast response of the neurons activated by the stimulus but also by integration of that activation over a noisy, contrast-dependent extent of the stimulus in space and time. Thus, when we wish to measure precisely the influence of spatial and temporal integration on threshold, we cannot do so by combining contrast threshold measures with Gaussian-windowed stimuli. © 1997 Optical Society of America. [S0740-3232(97)02201-1]

1. INTRODUCTION

Gaussian-windowed sinusoidal gratings have been used for a dizzying array of different experimental investigations, including measurements of our ability to combine motion information over visual space^{1,2} and specification of a motion stimulus to which our visual systems are most sensitive.³ These stimuli are often referred to as Gabor patches (or simply as a Gabor) after the mathematician who expounded particular theoretical advantages of the mathematical form.⁴ Gabor showed that this stimulus form minimized a certain measure of uncertainty of stimulus localization simultaneously in two domains: spatial frequency and (visual) space. This mathematical property has provided one theoretical motivation for the stimulus's use. Other advantageous properties include simple analytic expressions for the Gabor representation both in space and in spatial frequency. The general expression for a one-dimensional sinusoidal luminance grating that is Gaussian windowed in space is

$$L(x, y, t) = L_m \left\{ 1 + C_p \cos[2\pi x f_c + \theta_c(t)] \right. \\ \left. \times \exp \left[-\frac{1}{2} \left(\frac{x}{\sigma_x} \right)^2 - \frac{1}{2} \left(\frac{y}{\sigma_y} \right)^2 \right] \right\}, \quad (1)$$

where L_m is the mean luminance of the display, C_p is the peak contrast of the Gabor, f_c is the grating spatial frequency (the carrier), and σ_x and σ_y are the standard de-

viations of the spatial Gaussian window. The parameter $\theta_c(t)$ controls the change of position over time of the carrier. The spatiotemporally pointwise deviation of the stimulus luminance from the mean luminance is just $C(x, y, t) = L(x, y, t)/L_m - 1$. The stimulus allows independent control of the carrier spatial frequency, f_c , as well as the spatial size and frequency bandwidth determined by σ_x and σ_y . Moreover, a case has been made that the spatial profile of the stimulus is a good representation of simple cell receptive field profiles,^{5,6} although it may be that other mathematical forms are equally justifiable (cf. Refs. 7 and 8; also see Ref. 9).

These theoretical and physiological observations provide sufficient justification for many researchers who are interested in investigating the effects of stimulus spatial frequency and bandwidth and of spatial and temporal extent on visual phenomena. However, it is not clear which metric is appropriate for specifying the visual size (perceived spatial extent) of a Gabor. Often, Gaussian standard deviation is used as a metric, but to our knowledge there has been no direct measure of the correspondence between Gaussian standard deviation and the perceived visual extent of a Gabor patch. This lack of interest in the correspondence between standard deviation and perceived Gabor size is somewhat surprising because it is commonly known that the perceived size of a Gabor with a fixed standard deviation changes with its peak contrast [C_p in Eq. (1)]. This phenomenon is demonstrated in

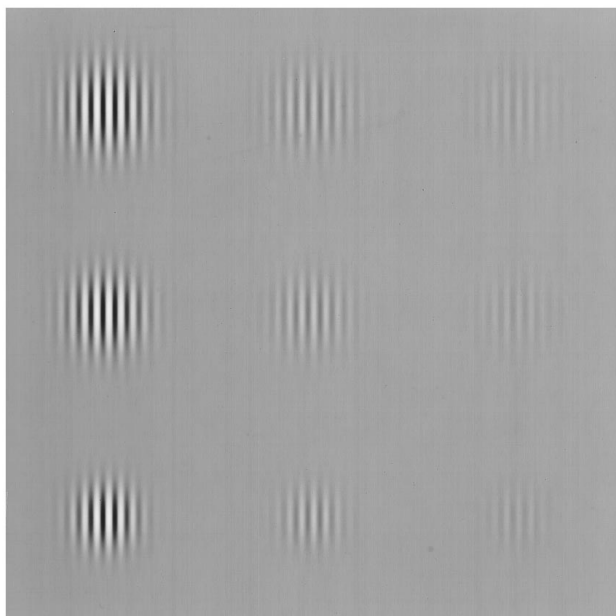


Fig. 1. Demonstration of the phenomenon of perceived Gabor size dependence on contrast. Gaussian standard deviation decreases from top to bottom, and peak contrast decreases from left to right. Contrast values (85%, 21%, 6%) were selected to produce approximately equal steps in perceived radius. Note that patches on rightward diagonals (e.g., bottom left to top right) have approximately equal apparent sizes.

Fig. 1; Gaussian standard deviation decreases from top to bottom, and peak contrast decreases from left to right.

It is therefore surprising that experiments employing Gabors to measure the influence of stimulus spatial extent on motion perception have used peak contrast as a threshold variable.¹⁻³ In general, if we wish to measure the influence of a stimulus parameter on some percept, then that parameter should be manipulated independently from other parameters. If the parameter of interest and the threshold parameter—in this case stimulus spatial extent and peak contrast—are not independent, then we must be certain how the two parameters are related in order to reach any conclusions.

It is clear that we need to understand how a stimulus's spatial area affects perception, but stimuli that are sharp edged and stimuli that are mathematically unlimited in size (e.g., a Gaussian window) have not been treated with the same size metric. However, we can move toward a single metric by considering how stimuli are processed by the visual system. Specifically, we will start with the assumption that perceived spatial extent and corresponding percepts are directly related to the cortical area activated by the stimulus. Figure 2 indicates how we might consider this situation with an abstract representation of how visual space is mapped to area V1 in primates.^{10,11} The figure shows a half-bull's-eye with logarithmically spaced concentric rings. Assuming fixation at the small circle at the center of the half-bull's-eye, Fig. 2(b) shows how the bull's-eye maps to V1 as indicated by 2-deoxyglucose experiments.¹¹ The paths in visual space represented by the arrows in Fig. 2(a) follow cortical paths as indicated in Fig. 2(b). The numbers in Fig. 2(b) provide a key to those paths, while their sizes indicate

schematically how visual area away from fixation is relatively expanded or compressed in the cortical representation.

Shapes in visual space are altered in the cortical mapping, but that mapping can be shown to be approximately conformal.¹² For example, a disk in visual space [Fig. 2(a)] maps to a nondisk in V1 [Fig. 2(b)] but remains contiguous because of the retinotopy that produces the conformal mapping. Conformal mapping properties should be all that is required for simple assumptions of object-shape processing because the processing machinery (the neurons) can be cortically arranged in the same coordinate system. For example, if we activate the same cortical region (position and extent) with two different stimuli, then the simplest expectation is that the stimuli are perceived to have the same visual spatial extent. Conversely, stimuli with different perceived spatial extents can be assumed to activate differing cortical extents. This provides the necessary context for asking the question, How much cortical area is activated by a stimulus? Specifically, we want a model of how a Gaussian-windowed stimulus activates neurons in cortex, with the assumption that perceived spatial extent is directly related to that activated cortical extent.

The stimulus specification provided by Eq. (1) is our starting point for such a model. Figure 3 shows a static

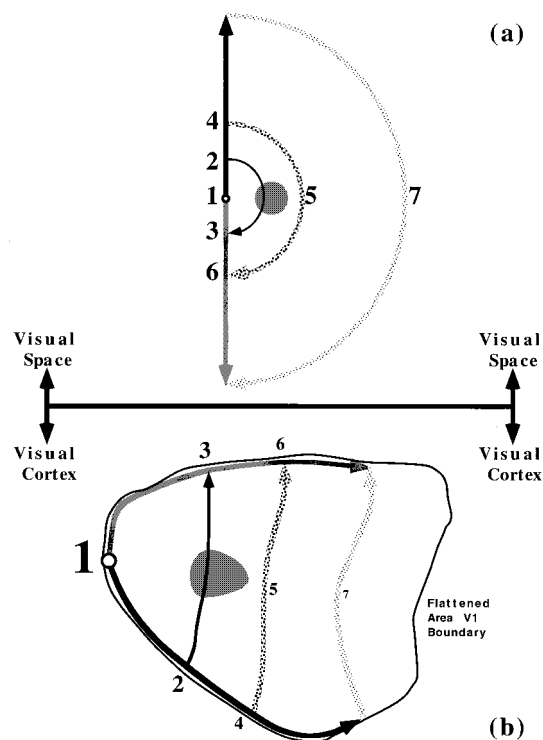


Fig. 2. Abstract representation of how visual space is mapped to area V1 in primates. (a) Half-bull's-eye with logarithmically spaced concentric rings. Assuming fixation at the small black circle at the center of the half-bull's-eye, (b) shows how the bull's-eye is mapped to V1 as indicated by 2-deoxyglucose experiments. The paths in visual space represented by the arrows in (a) follow cortical paths as indicated in (b). The numbers provide a key to those paths, while digit size indicates schematically how visual area away from fixation is relatively expanded or compressed in the cortical representation.

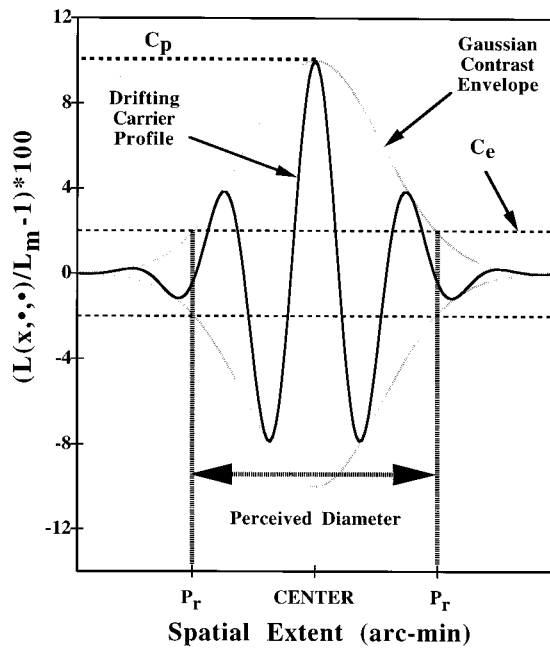


Fig. 3. Illustration of the working hypothesis. The Gaussian contrast envelope and the contrast-modulated, drifting sinusoidal carrier are shown together with a hypothetical contrast level (C_e) that limits visibility of the carrier. The perceived radius (P_r) indicated in the graph and in Eq. (2) is shown as the point at which the carrier contrast falls below C_e .

profile for $C(x, y, t)$, the pointwise deviation of stimulus luminance from the mean. We point out that with static gratings there are stimulus parameter combinations in which the phase of the static carrier can significantly change the size and the shape of the perceived patch (e.g., low carrier frequency relative to window size). Use of a drifting grating allows us to bypass questions concerning the perceived locations of the edges of the grating and of how that might alter the perceived size and shape. The drifting carrier sweeps past the region of the contrast-modulated window, activating neurons in the corresponding cortical area. In other words, the perceived spatial extent of the Gabor patch is defined not by the positions of the edges of the carrier but by the locations at which they appear and disappear as determined by the Gaussian window.

Cortical neurons will respond to the drifting grating with a magnitude that is a function of $C(x, y, t)$. Neuronal response to a stimulus is often modeled with the use of a function that first accelerates, then saturates; for example, a Naka-Rushton function such as $R(C) = MC^n / (K^n + C^n)$, where M is the saturated response magnitude and n is positive. Note that any such transformation of the Gaussian window in Fig. 3 will perturb the window but not topographically alter it: The cortical response profile remains convex (in a noiseless system).

When we quantify the mathematical size of a Gaussian (or Naka-Rushton transformed Gaussian), we must choose a metric, or fiducial level, to apply to the function because it is otherwise infinite. This is sometimes chosen to be the space constant, or the point at which its magnitude falls to $1/e$, or approximately 36.8%, of the peak. Alternatively, if we are interested in statistical

distributions, then the standard deviation of the Gaussian is chosen because it has intuitive meaning. However, these fiducial levels cannot explain our perception of Gabor size. We therefore hypothesize that the visible extent of the carrier must be limited by a cortical (physiological) response threshold. Pursuing this analysis in the cortical domain can require knowledge of the $R(C)$ parameters as well as cortical magnification, and perhaps a model of cortical detection. However, our analysis can be greatly simplified. Rather than transform our stimulus into a cortical domain, we can instead consider the cortical response threshold level in the spatiotemporal domain, i.e., by using $C(x, y, t)$: if $R(C)$ is invertible, we need only know C_e . This bypasses the question of $R(C)$ parameters, as well as the exact form of cortical magnification. Moreover, by carefully designing our experiments around a well-defined metric in the visual domain, we can avoid having to postulate a model of cortical response to, and detection of, the stimulus (e.g., Ref. 13).

With the hypotheses expressed in Fig. 3 we can make a few predictions and then proceed to measure psychophysically the perceived size of Gabor patches. We begin by modeling a noiseless system. A noiseless model works well for describing perceived size at suprathreshold peak contrasts, but systemic noise significantly affects perceived Gabor size near contrast threshold. The influence of systemic noise will be accounted for in Section 5 by the use of a simple extension of the model. From Eq. (1) and Fig. 3 the perceived radius of a Gaussian-windowed drifting grating in a noiseless system is defined as

$$C_e = C_p \exp\left[-\frac{1}{2}\left(\frac{P_r}{\sigma}\right)^2\right], \quad (2)$$

where P_r is the perceived radius of the circular Gabor, C_e is the value of the Gaussian at the perceived edge of the Gabor, C_p is the Gabor peak contrast, and σ is the standard deviation of the patch in arcminutes. From this we can calculate the perceived radius as

$$P_r = \sigma \sqrt{-2 \ln\left(\frac{C_e}{C_p}\right)} \quad (\text{arcmin}). \quad (3)$$

The equation says that if we fix the peak contrast of the Gabor, then we should find linear variation of perceived radius with the standard deviation of the Gaussian envelope. However, if we fix the Gaussian standard deviation, then we should have a nonlinear but monotonic relationship between perceived radius and peak contrast. The resulting psychophysical data show that, as predicted, the perceived radius of a circular Gabor patch¹⁴ with a drifting carrier varies linearly with standard deviation but nonlinearly and monotonically with peak contrast. Perceived radius varies nonlinearly and nonmonotonically with carrier spatial frequency, as would be predicted from previous spatial frequency contrast threshold data.

After fitting Eq. (3) to the data, we find that they are well described by a two-parameter model in which C_e also depends on the peak contrast (C_p) of the Gabor, as would be expected from the influence of (local) contrast gain control. This C_p -dependent threshold represents a type of self-masking. A comparison of values of C_e predicted by

the model with measures of contrast detection threshold for the stimulus indicate that the two are not distinguishable: C_e must be very near to, or the same as, contrast threshold. We conclude that measures of contrast threshold using Gaussian-windowed stimuli are determined not just by contrast response of the neurons activated by the stimulus but also by an integration of that activation over a noisy, contrast-dependent extent of the stimulus in cortex (space) and time. This conclusion has bearing on experiments that require that contrast thresholds be independent of other stimulus parameters.

2. METHODS

A. Apparatus

Visual stimuli were displayed on a Nanao Flexscan 6500 monitor (Eizo Nanao Technologies, Torrance, Calif.) with the use of a Cambridge Research Systems graphics card model VSG 2/3 (Cambridge Research Systems, Ltd., Rochester, Kent, England) with 4 Mbytes of video memory. The VSG 2/3 has built-in hardware for pseudo-12-bit resolution through a linear combination of two 8-bit digital-to-analog converters. Pseudo-12-bit resolution allows the use of 256 levels taken from a possible range of 4096 levels and permits fine luminance resolution when only a small luminance range is required. The digital-to-analog converter combination method allows the use of 256 luminance values in the range $L_0(1 \pm m)0.0625$, where L_0 is the display's mean luminance and m is an integer from 1 to 16. The smallest compatible contrast range was used in each experiment presented here. For example, a 7% peak contrast stimulus was presented with the use of a contrast range of 12.5% ($m = 2$), so the contrast resolution was just less than 0.1%. The display was gamma corrected and linearized for pseudo-12-bit resolution with the use of a United Detector Technologies model S370 photometer (Graseby Optronics, Orlando, Fla.). The monitor ran at 100-Hz vertical refresh rate and had a mean luminance of 20.5 cd/m². The display area was 22.5 × 22.5 cm (512 × 512 pixels) square and viewed from 80 cm, producing a display area of 16 × 16 deg.

B. Experimental Method

The method of constant stimuli was used to measure a point of subjective equality for perceived size of Gabor patches with a drifting carrier. On any trial the subject viewed the display binocularly and was first presented with a fixation point in the center of the screen. Removal of the fixation point and presentation of the stimulus were initiated by a key press on the host computer for the graphics card. The test stimulus was composed of a circular Gabor (i.e., $\sigma_x = \sigma_y$) and a positive-increment contrast disk. Comparison disks were circular with edges defined by step functions of 7% contrast, thereby providing a sharply defined cortical activation area to which we can compare the Gabor. Pilot experiments indicated that circular disks of higher and lower contrasts were perceived as the same size as that of the 7% contrast disk. The two images were presented 2.7 deg (86 pixels) to either side of the fixation point on the horizontal meridian. The disk and Gabor center x and y positions on the screen were both randomly jittered by an amount chosen uni-

formly from the interval ± 0.19 deg (± 6 pixels). The side of presentation of the Gabor and the disk, and the direction of drift of the carrier (leftward or rightward), were randomized for each trial. Stimuli were always presented for 0.5 s with abrupt onset and offset. The subject's task was to select the image (either Gabor or disk) that appeared larger. Each data point presented here consists of at least 150 trials over at least five sizes of disk. Conditions were not interleaved, on account of equipment limitations. A cumulative Gaussian function was fitted to the psychometric data for each condition with the use of a maximum-likelihood procedure. The fit estimated the mean and the standard deviation of the Gaussian, as well as the 95% confidence intervals for each parameter by use of appropriate χ^2 error surface contours.¹⁵

C. Gabor Stimulus Generation

Gabor luminance profiles were defined as in Eq. (1) and were presented in a square temporal contrast window (i.e., abrupt onset and offset). All Gabor patches and reference disks were generated before the experimental session and stored in the video random access memory of the VSG card. Drifting stimuli were generated as a sequence of 12 images with phase relationships defined as $\theta_c(n) = 2\pi n/12$ for n between 0 and 11. This produced a spatial displacement of 30 deg of the carrier between each image in the sequence. The sequence was presented one image every four video frames (40 ms) to produce a drift rate of 2.08 cycles of the carrier per second. The initial carrier phase was randomized for each presentation.

3. RESULTS

Two subjects (two of the authors) measured points of subjective equality (perceived Gabor radius, P_r), using standard deviations of 7, 10, 14, 21, and 28 pixels (13.125, 18.75, 26.25, 39.375, and 52.5 arcmin, respectively) at 2%, 3.5%, 7%, 14%, 28%, and 56% peak contrast and at 0.1, 1, 3, and 6 cycles/degree (cpd). The data are shown in Fig. 4. Some of the lowest-peak-contrast and smallest-standard-deviation values were not measurable. Some of these patches were not visible, while others could be detected but their characteristics were not perceptually well defined. Perceived Gabor radius is plotted against Gaussian standard deviation, with peak contrast as a parameter in each graph. Data for both subjects are shown in graph pairs, with the spatial frequency for each condition indicated in each graph. The typical 95% confidence interval for all data points ranged from ± 1 arcmin for the smallest standard deviation to ± 2 arcmin for the largest standard deviation. No error bars are shown because they are typically smaller than the size of the symbols.

Figure 4 shows that the perceived radius (P_r) of the Gabor varies linearly with the standard deviation of the Gaussian envelope. However, the slope of that variation, $\partial P_r / \partial \sigma$, can vary from almost 3 to almost 1, depending on the spatial frequency and the peak contrast of the Gabor. As peak contrast decreases, $\partial P_r / \partial \sigma$ also decreases. Moreover, $\partial P_r / \partial \sigma$ clearly depends on the spatial frequency of the carrier, being higher for 1 and 3 cpd than for 0.1 and 6 cpd. In order to quantify the linearity of the

slope, we found linear fits to each data curve in Fig. 4. The y intercept of that fit varied near zero in an unsystematic manner, and the r^2 goodness of fit was always 0.974 or higher, with most values at 0.99 or higher. This result, combined with the consistency of the 95% confidence interval for each data point, stresses the high degree of linearity of the data with Gaussian standard deviation. Note that the greatest deviation from linearity is at low peak contrasts for the 3- and 6-cpd data. This should be expected because contrast threshold variation with position in the visual field is larger for higher spatial frequencies. That threshold variation with position is not included in the model and will therefore lead to some error at higher carrier frequencies on account of parafoveal viewing.

4. EVALUATING THE CONTRAST THRESHOLD MODEL

Calculating the Gaussian height at the perceived Gabor edge, C_e , by using Eq. (2) for each estimate of P_r indicates that Eq. (2) is not quite correct: C_e varies with the peak contrast (C_p) of the Gabor. There was some variation of C_e with standard deviation (σ) of the Gabor, but that variation was not systematic across subjects or spatial frequencies. Fitting the data, including variation of C_e with σ , showed that the variation is not statistically different from zero for six of the eight data sets (two ob-

servers at four spatial frequencies). For this reason we chose to fit the perceived radius data by using a threshold described by $C_e = K_0 + C_p K_1$, which includes a linear variation of C_e with C_p . Combining this model of C_e with Eq. (2) produces

$$C_e = K_0 + C_p K_1 = C_p \exp\left[-\frac{1}{2}\left(\frac{P_r}{\sigma}\right)^2\right] \quad (4)$$

or, explicitly,

$$P_r = \sigma \sqrt{-2 \ln\left(\frac{K_0 + C_p K_1}{C_p}\right)} \quad (\text{arcmin}). \quad (5)$$

The rate of change of perceived radius with standard deviation is therefore given by

$$\frac{\partial P_r}{\partial \sigma} = \sqrt{-2 \ln\left(\frac{K_0 + C_p K_1}{C_p}\right)} \quad (\text{arcmin})/(\% \text{ contrast}). \quad (6)$$

Because the data show that $\partial P_r / \partial \sigma$ changes with spatial frequency, we fit the data in groups by spatial frequency, using Eq. (5) and a least-squared-error method. The data from Fig. 4 are replotted in Fig. 5 against peak contrast, together with the fitted curves. The data for subject EF are shown with open symbols, while the data for subject PB are shown with filled symbols. The fitted curves for EF are shown with solid curves, while the fitted curves for PB are shown with dashed curves.

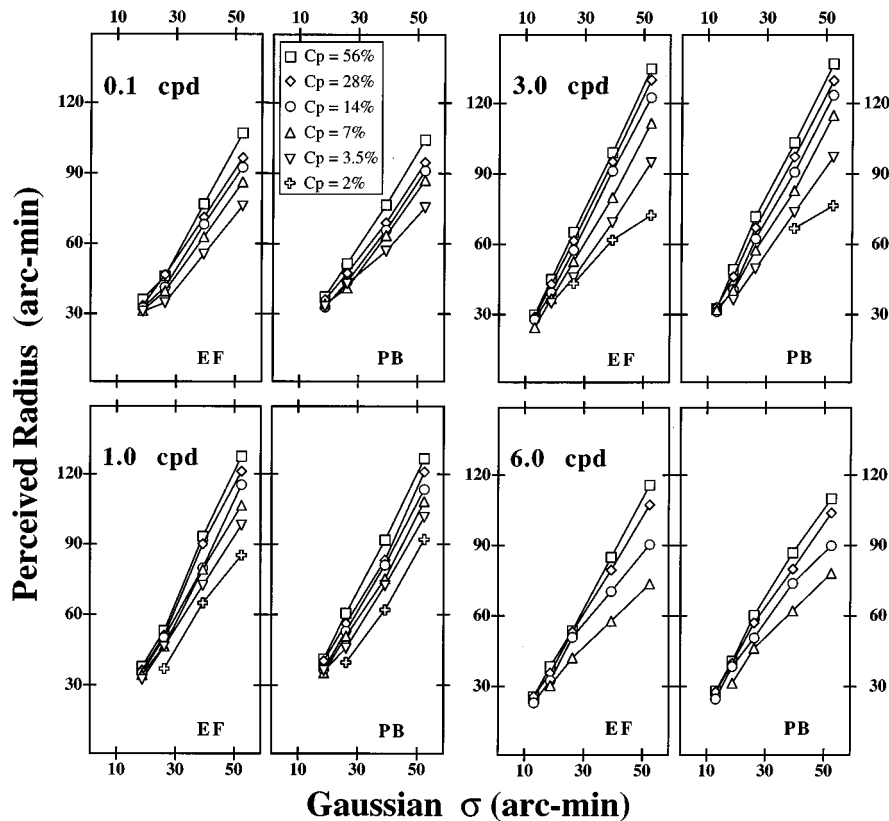


Fig. 4. Perceived Gabor radius plotted against Gaussian standard deviation, with peak contrast (values shown in the legend) as a parameter in each graph. The data for both subjects are shown in graph pairs, with the spatial frequency for each condition indicated in each graph. The typical 95% confidence interval for all data points ranged from ± 1 arcmin for the smallest standard deviation to ± 2 arcmin for the largest standard deviation. No error bars are shown because they are all smaller than the size of the symbols.

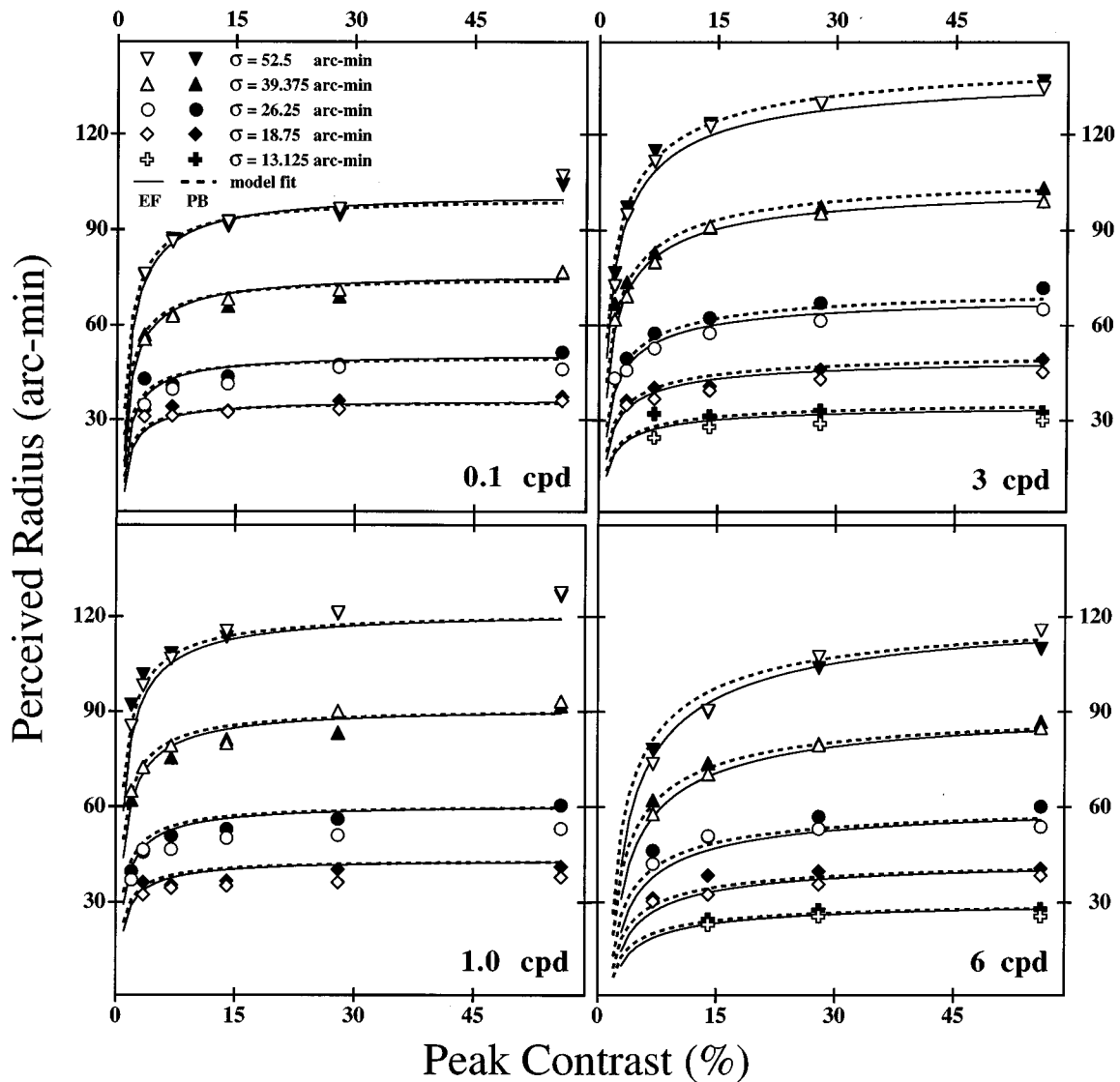


Fig. 5. Data from Fig. 4 replotted against peak contrast, together with the curve fits from the use of Eq. (5). The data for subject EF are shown with open symbols, while the data for subject PB are shown with filled symbols. The fits for EF are shown with solid curves, while the fits for PB are shown with dashed curves.

Table 1 details the fitted parameter values, their 95% confidence limits, and goodness-of-fit statistics for each observer for each spatial frequency. A true χ^2 measure cannot be calculated because the confidence intervals on individual data points do not include experimental error across conditions. The coefficient of determination (COD) indicates that from 97.8% to 99.5% of the data variance is accounted for by just two parameters. However, the serial correlation values imply a real deviation of the model from the data and hence underparameterization of the model. Inspection of the error surfaces indicates that the systematic deviation of the model from the data is not consistent across spatial frequency conditions. Attempts to modify the model further based on error surface information failed in that no tested modification produced consistent fit improvements or consistently nonzero parameter values across spatial frequencies and subjects.

A. Interpreting the Model Parameters

K_0 represents C_e if the presence of the stimulus does not affect detection (see the interpretation of K_1 below). The values and the variation of K_0 are consistent with the known variation of contrast threshold with spatial frequency, increasing from 0.1 to 3 cpd and then decreasing at 6 cpd. Comparison of perceived radius across spatial frequency for fixed contrast and standard deviation shows a corresponding dependence on spatial frequency. Figure 6 plots perceived Gabor radius data for contrast values of 3.5%, 7%, 14%, 28%, and 56% for a standard deviation of 21 pixels (39.4 arcmin) across spatial frequency. Some of the data are taken from Fig. 4, while the data for 0.3 and 0.6 cpd were additionally measured for completion of the curves. The graph clearly shows that perceived radius of a Gabor of otherwise fixed parameter values depends on spatial frequency. Moreover, the

variation of the size dependence with spatial frequency is consistent with the known behavior of contrast thresholds across spatial frequency. The correspondence confirms that higher sensitivity to the carrier produces a larger perceived Gabor radius.

Without K_1 [i.e., if we used Eq. (2)] the goodness of fit as indicated by the r^2 value is still very good (of the order of 0.95), but the model selection criterion (MSC), a more sensitive measure of error-variance reduction, is much lower. Model fits with constant C_e , i.e., with $K_1=0$, produce more error for the low-contrast data (i.e., leftmost points in Fig. 5). The requirement for K_1 in the fit can be interpreted: K_1 corresponds to an increase of C_e as peak Gabor contrast is increased. It has been previously shown that stimulus contrasts as low as 3% can change neuronal response gain, even doubling the neuronal response threshold.^{19,20} We therefore interpret the presence of K_1 as representing the influence of contrast gain control that produces self-masking. That is, the presence of the high-contrast center region of the Gabor effectively increases C_e because contrast gain is reduced. Increasing the Gabor peak contrast increases the area of the Gabor above threshold but also incrementally increases the local threshold slightly, so the perceived size of the patch does not increase quite as much as would be expected from a constant, absolute threshold.

This phenomenon may also be related to apparent contrast; when the apparent contrast of a patch of grating is measured with the use of a matching paradigm, the

patch's apparent contrast is reduced when it is spatially adjacent to or surrounded by a high-contrast region of grating.²¹ This observation is related to the slope of the Gaussian envelope at the perceived edge of the Gabor patch (the data are not shown). The slope of the Gaussian envelope is a measure directly related to the nearness of the high-contrast center to the perceived Gabor edge, or the low-contrast surround of the Gabor. Lower values of C_e are matched to lower envelope slopes, which correspond to larger distances from the high-contrast center of the Gabor. In a like manner, reduction of apparent contrast of a test patch of grating decreases with the distance from an adjacent high-contrast grating.²¹

B. C_e and Contrast Detection Threshold

As shown by the goodness-of-fit measures in Table 1, the model fits the data very well. Moreover, although the model is not intended to be a model of contrast detection threshold, we can seek extra support for the model by using it to predict contrast thresholds and comparing those predictions with measured thresholds. We note that extrapolation beyond measured data (i.e., down to threshold) can be error prone, but the fits and the parameter estimates are good enough to support this action. Both subjects measured contrast detection performance by using a two-alternative-forced-choice procedure on the same equipment and software as those for the measurements of perceived radius. The sharp-edged disk was removed from the display, and the observer's task was to

Table 1. Fitted Parameters for Eq. (4) for Each Subject for Each Spatial Frequency, Together with a Statistical Analysis of the Goodness of Fit^a

Parameter Values for Each Subject	K_0 (% Contrast)	K_1 (% Contrast/% Contrast)	N	SC	σ_e (arcmin)	Σe^2 (arcmin ²)	r^2	COD	MSC
EF									
0.1 cpd (95% interval)	0.777 [0.551, 1.00]	0.152 [0.126, 0.178]	20	2.16	2.96	160	0.998	0.986	4.07
1.0 cpd (95% interval)	0.437 [0.295, 0.580]	0.0678 [0.0476, 0.0880]	23	2.94	4.65	455	0.997	0.978	3.65
3.0 cpd (95% interval)	0.608 [0.531, 0.685]	0.0309 [0.0232, 0.0386]	27	1.14	2.6	169	0.999	0.994	4.97
6.0 cpd (95% interval)	1.997 [1.646, 2.348]	0.0619 [0.0429, 0.0810]	19	0.53	2.36	95	0.999	0.993	4.81
PB									
0.1 cpd (95% interval)	0.657 [0.427, 0.886]	0.160 [0.133, 0.187]	20	1.51	3.10	173	0.998	0.983	3.84
1.0 cpd (95% interval)	0.385 [0.278, 0.492]	0.0688 [0.0530, 0.0845]	23	2.84	3.67	282	0.998	0.985	4.04
3.0 cpd (95% interval)	0.543 [0.479, 0.672]	0.0241 [0.0182, 0.0300]	27	1.20	2.29	126	0.999	0.995	5.19
6.0 cpd (95% interval)	1.62 [1.182, 2.063]	0.0705 [0.0455, 0.0956]	19	2.50	3.13	166	0.998	0.987	4.12

^a Each best-fit parameter value appears together with its 95% confidence interval determined by a search of the error surface for an appropriate contour level.¹⁶ The number of data points (N) in each fit is presented together with the serial correlation (SC), the standard deviation of the model error (σ_e), and the total squared error (Σe^2). Last, we provide three goodness-of-fit measures: r^2 , the coefficient of determination (COD), and the model selection criterion (MSC).¹⁷ Each is a successively more sensitive metric for how well the model accounts for the variance of the data. The MSC also accounts for extra degrees of freedom resulting from increased parameter count and is derived from the Akaike information criterion.¹⁸ In summary, the MSC is calculated as $\ln(A/B) - 2p/N$, where N is the number of data points, p is the number of model parameters, A is the sum of weighted, squared deviations of the data from the weighted mean of the data, and B is the sum of weighted, squared deviations of the data from the model. Larger values indicate a better fit. For example, a MSC of 5.19 (subject PB, 3 cpd) indicates an A/B ratio of 208.

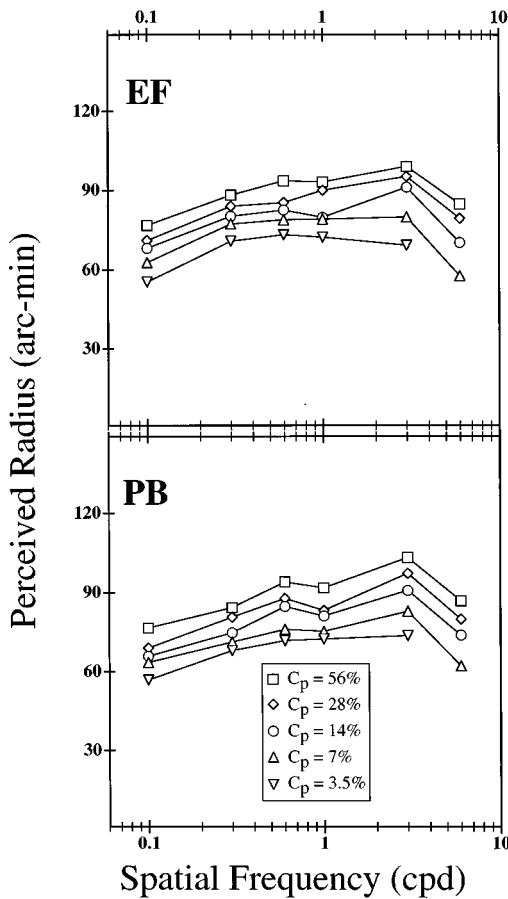


Fig. 6. Perceived Gabor radius data for contrast values of 3.5%, 7%, 14%, 28%, and 56% for a standard deviation of 21 pixels (39.4 arcmin) across spatial frequency. Some of the data are taken from Fig. 2, while the data for 0.3 and 0.6 cpd were additionally measured for completion of the curves. The graph clearly shows that perceived radius of a Gabor of otherwise fixed parameter values depends on the spatial frequency of the carrier.

detect the side of the display upon which the drifting Gabor appeared. Performance was measured for each of the four spatial frequencies with the use of a method of constant stimuli and a Gaussian standard deviation of 52.5 arcmin. In the noiseless model perceived size goes to zero when $C_p = C_e$ [or $C_p = K_0 / (1 - K_1)$]. As explained in Subsection 5.C in the extension of the model to include noise near and at threshold, if C_e is the same as contrast detection threshold for the carrier, then detection likelihood is 75% correct when $C_p = C_e$. We therefore measured 75% correct thresholds by fitting a cumulative normal function to the detection data with a maximum-likelihood method. Model predictions of contrast threshold were calculated as $C_{th} = K_0 / (1 - K_1)$ from Table 1.

Figure 7 plots the measured thresholds (cross-filled symbols) against predicted thresholds (open symbols). 95% confidence intervals are added to the model predictions with the use of the 95% confidence intervals for K_0 and K_1 . Subject PB's data are shifted downward by 10 dB for clarification of the figure. Only one point per subject can be rejected as different from the prediction. Those two points occur for the two spatial frequencies that contain fewer low-peak-contrast data to constrain

the steepest-sloping part of the model, the segment that must be accurate if the model is to predict threshold well. An additional source of error that could influence the 6-cpd predictions is that the model does not include any influence of the variation of contrast threshold with position in the visual field. That variation is larger for higher spatial frequencies. The success of these model predictions supports the conclusion that if C_e is different from contrast detection threshold for the drifting carrier, that difference is not visible in our results. We therefore accept the hypothesis that C_e and contrast detection threshold are the same.

C. Observations

Our experiences in this study compel us to make an observation that seems to be contrary to popular opinion. Because a Gabor has a Gaussian contrast envelope, it is often referred to as a fuzzy stimulus, in that the edges of the patch are not perceptually well defined. The data presented here specifically show that, consistent with a previous report of our ability to categorize disk size,²² our perception of the size of a Gabor is not fuzzy in any way. The 95% confidence intervals derived from the psychometric functions are extremely sharp, being from ± 1 for $\sigma = 13.125$ arcmin to ± 2 for $\sigma = 52.5$ arcmin. Moreover, we can use the standard deviations derived from the psychometric functions to estimate a Weber fraction for the Gabor. The standard deviation of the fitted cumulative normal indicates that we regularly see the disk as different in size from the Gabor when it is 5%–6% larger or smaller (depending on the observer) than the perceived size of the Gabor. This value is well within the expected

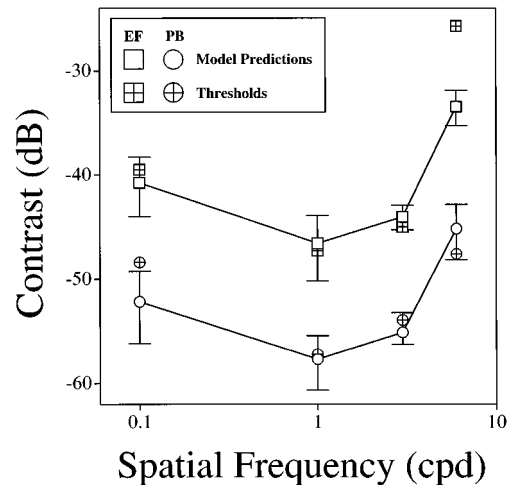


Fig. 7. Measured contrast detection thresholds (cross-filled symbols) together with model predictions (open symbols). 95% confidence intervals are added to the model predictions with the use of the 95% confidence intervals for K_0 and K_1 . Subject PB's data are shifted downward by 10 dB for clarification of the presentation. Only one point per subject can be rejected as different from the prediction. Those two points occur for the two spatial frequencies that contain fewer low-peak-contrast data to constrain the steepest-sloping part of the model, the segment of the model curve that must be accurate if it is to predict threshold well.

range for Weber fractions in other tasks. The Weber fraction is lower for the middle spatial frequencies and for higher contrasts.

5. DISCUSSION

A. Comparison with Previous Work

Gelb and Wilson,²³ in a study similar to the present one, measured the perceived size of spatially narrow-band difference of Gaussian (DOG) patterns. Their metric stimulus, or standard, was held constant at 50% peak contrast (peak divided by the mean, as in our study). Complementary to our approach, their method of measuring a point of subjective equality was to vary the size of the DOG of interest rather than that of the standard. The DOG of interest was fixed to a lower contrast, and then they varied its σ in a double Cornsweet-staircase procedure to find the value of σ that produced a perceived size equal to that of the standard. The task was performed for a number of DOG contrast values and for different values of σ for the standard. They explained the resulting perceived size data by using a model containing four spatial frequency channels, or mechanisms, which have nonlinear contrast response functions. The mechanism outputs were linearly weighted, summed, and normalized to produce a size index related to the relative strengths of response from each spatial frequency channel. They found that this model could reproduce the shapes of some but not all of their data curves. Those data varied across subjects and depended on contrast in an inexplicable manner. Moreover, the absolute perceived sizes of their DOG patterns were never measured because the absolute sizes of the standards were never determined.

Our intent is not to investigate any internal metric of object size, although Gelb and Wilson²³ were apparently attempting to capture such an internal metric with their model. However, we also believe that they were measuring the same phenomenon that we have measured, albeit in a complementary manner. Our results and model appear to explain the unexpected behaviors of their data. We must first realize that as the standard deviation of their test (the lower-contrast DOG) increased, its peak spatial frequency (f_p) decreased as given by [their Eq. (2)]

$$f_p = \frac{0.2564}{\sigma} \quad (\text{cpd}). \quad (7)$$

During their staircase procedure their stimulus simultaneously moved across the dimensions of mathematical size (as determined by their σ) and spatial frequency. Figure 6 clearly shows that the dependence of perceived size on spatial frequency (at least, in our Gabor patches) is not monotonic. Changing the spatial frequency can either increase or decrease the perceived size of the patch, depending on the peak frequency of the DOG. This phenomenon can result in opposing forces on the perceived size of the Gabor; decreasing σ tends to decrease the perceived size, but increasing spatial frequency can increase its perceived size.

This property can explain the situation in which Gelb and Wilson's medium-frequency (less than 3 cpd), medium-standard-deviation DOG standards were matched to smaller-standard-deviation DOGs. Increas-

ing stimulus spatial frequency by reducing standard deviation increased sensitivity to the stimulus enough to increase its perceived size faster than its perceived size was reduced by the standard deviation. This would be most prominent at low contrasts, where the variation of perceived size is slowest with standard deviation (see Fig. 4) and the reduction of σ could be easily countered by an increase of spatial frequency.

B. Implications for Previous Work

The data presented here indicate that varying the peak contrast of the Gaussian envelope can significantly change the perceived radius of the Gabor. We can directly extend this spatial phenomenon to the temporal domain (supported by observation): Temporally Gaussian contrast windows cause perceived patch size to change with time, first increasing and then decreasing. Detection thresholds must depend on the spatiotemporally integrated response of cortical neurons. We therefore conclude that contrast thresholds measured with the use of a spatiotemporally Gaussian contrast envelope result from integration of neural response over a contrast-dependent corticotemporal volume.²⁴ Note that although square-edged, flat-topped contrast windows (e.g., Refs. 25–28) may produce slightly more frequency spread than a Gaussian, they do not suffer from this problem.

Anderson and Burr^{1,2} explored the influence of spatial integration area on motion perception by measuring contrast thresholds for direction discrimination for a number of Gabor spatial frequencies and by using standard deviation as the size metric. The change of measured threshold with stimulus size is taken to implicate the underlying detector–output combination function. However, what we need to know here is the activated cortical area at threshold. We perform this analysis in the context of a noiseless system, but in Subsection 5.C we discuss the consequences of a noisy system on perceived size at threshold. Figure 8 shows a graph of the derivative of

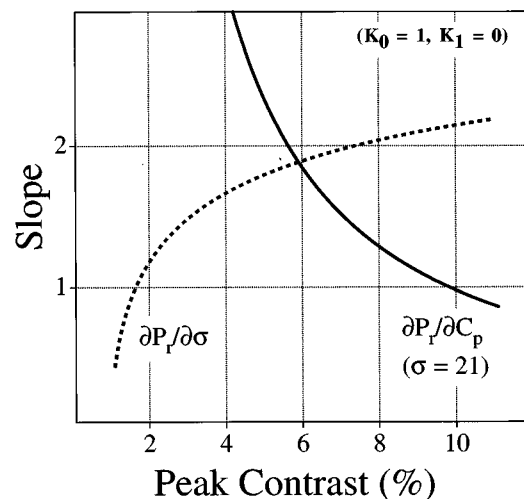


Fig. 8. Derivative of perceived radius with respect to contrast ($\partial P_r / \partial C_p$, shown by the solid curve) for a standard deviation of 21 and derivative of perceived radius with respect to standard deviation [$\partial P_r / \partial \sigma$ given by Eq. (6), shown by the dashed curve]. In both cases we have set $K_0 = 1$ and $K_1 = 0$ for convenience.

perceived radius with respect to contrast ($\partial P_r/\partial C_p$, shown by the solid curve) for a standard deviation of 21 and the derivative of perceived radius with respect to standard deviation [$\partial P_r/\partial \sigma$ given by Eq. (5), shown by the dashed curve]. In both cases we have set $K_0 = 1$ and $K_1 = 0$ for convenience, although the qualitative results are the same if we use other parameter values. Note that the upper (horizontal) asymptote for $\partial P_r/\partial \sigma$ is given by $\sqrt{-2 \ln K_1}$, the left-hand (vertical) asymptote is at $C_p = K_0$, and $\partial P_r/\partial \sigma$ is undefined when $C_p < K_0/(1 - K_1)$.

Figure 8 shows that as contrast is reduced in this noiseless model, $\partial P_r/\partial \sigma$ decreases. Note that $\partial P_r/\partial \sigma = 1$ only at a peak contrast of 1.64%, or 4.3 dB above threshold. (The threshold for this condition is determined by both K_0 and K_1 .) As C_p approaches threshold (C_{th} ; in this case 1%), $\partial P_r/\partial \sigma$ rapidly goes to zero. For a fixed σ , $\partial P_r/\partial C_p$ (solid curve) varies in a complementary manner. Near threshold $\partial P_r/\partial C_p$ is enormous. At 2% contrast (6 dB above threshold) $\partial P_r/\partial C_p$ is larger than 8. At 1.1% contrast (0.8 dB above threshold) $\partial P_r/\partial C_p$ is over 30. The impact of this change on cortical activation area is even more drastic because it is proportional to the square of the perceived radius. With the use of Eq. (4) the perceived area (P_a) of the patch is

$$P_a = \pi \sigma^2 \left[-2 \ln \left(\frac{K_0 + C_p K_1}{C_p} \right) \right] (\text{arcmin})^2, \quad (8)$$

and the rate of change of perceived area ($\partial P_a/\partial C_p$) with Gabor peak contrast is

$$\frac{\partial P_a}{\partial C_p} = \frac{2\pi\sigma^2 K_0}{C_p K_0 + C_p^2 K_1} (\text{arcmin})^2 / (\% \text{ contrast}). \quad (9)$$

Clearly, $\partial P_a/\partial C_p$ is nonlinear in both standard deviation and peak contrast. Likewise, it is clear that using a Gaussian-windowed stimulus in combination with a contrast threshold does not give us direct information on how spatial summation area affects motion perception. At threshold there must be some amount of activation in the cortical neurons at the center of the Gabor patch representation, but the cortical extent of that activation is unknown. Moreover, that cortical activation extent changes with spatial frequency of the carrier (i.e., Fig. 6). Thus the influence of spatial frequency, stimulus duration, stimulus contrast, and spatial extent are confounded in the corticotemporal (spatiotemporal) integration volume.

C. Systemic Noise and Perceived Size at Threshold

Equations (5) and (8) predict that, in a noiseless system, perceived radius and area of a Gabor patch approach zero at detection threshold [$C_p = C_{th} = K_0/(1 - K_1)$]. However, it is clear that at contrast levels normally referred to as threshold we regularly see the stimulus as being non-zero in size. When we measure thresholds at, say 75% correct in a two-alternative-forced-choice procedure then we are actually correctly detecting the stimulus 50% of the time. That is, half of the time we can see the stimulus, and the other half of the time we guess with 50% accuracy. We can easily explain this phenomenon by extending the model to include noise that must be present

in the system. The systemic noise is conceptually consistent with a threshold that fluctuates (is noisy). Of course, the noise could be in the contrast gain control mechanism, and/or in the response of the neuronal population, and/or in the peak contrast (C_p) of the Gabor patch. If the noise fluctuations are small enough not to affect the contrast gain control, then these situations are mathematically similar. For this reason and for purposes of simplified exposition we model peak contrast of the Gabor as including a zero-mean random variable, \tilde{n} , with a probability-density function (PDF), $\rho_{\tilde{n}}$. This modifies our model of perceived radius to be

$$C_e = (C_p + \tilde{n}) \exp \left[-\frac{1}{2} \left(\frac{P_r}{\sigma} \right)^2 \right], \quad (10)$$

$$P_r = \sigma \sqrt{-2 \ln \left(\frac{C_e}{C_p + \tilde{n}} \right)} (\text{arcmin}). \quad (11)$$

Figure 9 shows how this form of systemic noise affects perceived size at and near detection threshold. Given a peak contrast exactly at threshold, the noise forces the Gabor below threshold 50% of the time and above threshold 50% of the time. In a two-alternative-forced-choice procedure we guess correctly half of the time that the Gabor is below threshold, resulting in detection performance at a 75% correct level. Moreover, the steep slope of the perceived radius function, $P_r(C_p)$ [dashed curve in Fig. 9(a)], with peak contrast implies that when the patch is above threshold, it will also appear to be relatively large. We can transform the PDF of \tilde{n} , $\rho_{\tilde{n}}$ [solid curve in Fig. 9(a)], to produce a PDF for perceived radius, $\rho_{\tilde{P}_r}$ [circles, in Fig. 9(a)], for the stimulus at contrast threshold. The appropriate theorem²⁹ is

$$\rho_{\tilde{P}_r} = |\partial C_p/\partial P_r| \rho_{\tilde{n}} [C_p(P_r)], \quad (12)$$

where $C_p(\cdot)$ is the function that maps P_r onto C_p [i.e., solve Eq. (4) for C_p]. Figures 9(b) and 9(c) show how changes in C_p or in the noise variance affect perceived size when the Gabor is above threshold. Note that the PDF's shown in Figs. 9(b) and 9(c) may not sum to 1.0 because they do not include the probability of the Gabor being below threshold; that case would be represented by a discrete probability category at $P_r = 0$, but inclusion of that category complicates the plots. For example, in Fig. 9 we assume that the noise is Gaussian distributed on a logarithmic contrast axis. The results indicate that, consistent with our data observations, increasing C_p should result in perceived sizes with less uncertainty (in terms of the Weber fraction for discrimination), while greater noise variance at threshold produces larger average perceived sizes (when the stimulus is seen). The latter is consistent with the observation that, at threshold, when we see the stimulus, it appears relatively large. For example, when σ of the Gaussian window is 14 arcmin and the noise standard deviation is 2.7 dB (the average σ of detection thresholds in Fig. 7), the average perceived diameter (when the Gabor is visible) is 16.5 arcmin and is larger than 20 arcmin 32% of the time. In a noiseless system the perceived size approaches zero at threshold, but noise in the system changes the perceived size into a stochastic process at and near threshold. We do not see

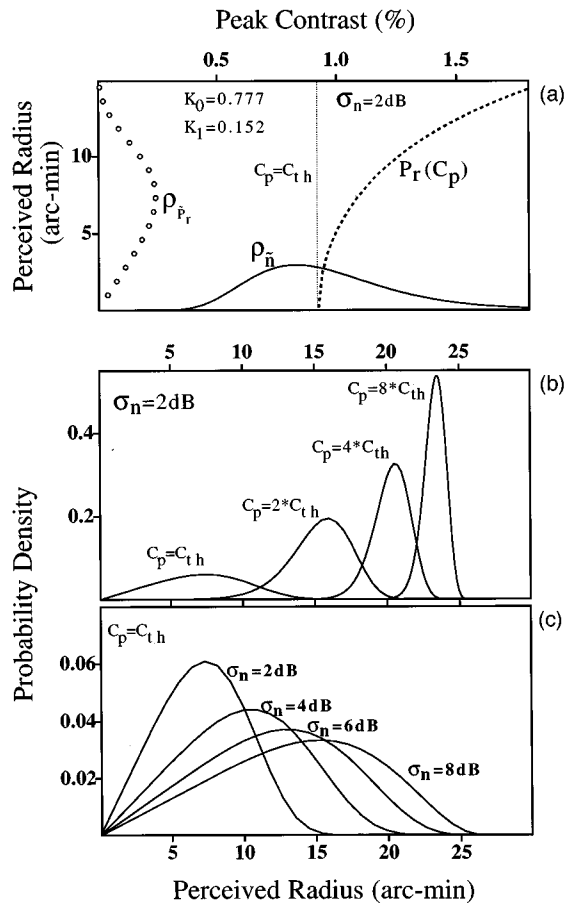


Fig. 9. Plot (a) shows how systemic noise combined with the perceived radius curve, $P_r(C_p)$, determines perceived size at threshold. The curve at the bottom of (a) is an example of a PDF, $\rho_{\bar{n}}$, which is Gaussian distributed on a logarithmic C_p axis. The PDF and $P_r(C_p)$ parameters are given in (a); K_0 and K_1 are from the 0.1-cpd condition for subject EF (see Table 1). The PDF for perceived size, $\rho_{\bar{r}}$, is shown at the left of (a). Only the portion of $\rho_{\bar{n}}$ to the right of the vertical line marking C_{th} is transformed to produce $\rho_{\bar{r}}$. The portion of $\rho_{\bar{n}}$ to the left of C_{th} represents conditions that are not visible and map to $P_r = 0$ (not shown for clarity). Both $\rho_{\bar{n}}$ and $\rho_{\bar{r}}$ have been scaled in magnitude for purposes of clarity. Note that the $\rho_{\bar{r}}$ curve in (a) and the left-hand curves in (b) and (c) are identical [except for a scaling in (a)] because they are the same condition: $C_p = C_{th}$ and $\sigma_n = 2$ dB. Plot (b) shows how $\rho_{\bar{r}}$ changes as C_p increases for fixed variance of $\rho_{\bar{n}}$. Note that as C_p increases, the variance of $\rho_{\bar{r}}$ decreases. Plot (c) shows how $\rho_{\bar{r}}$ changes as the variance of $\rho_{\bar{n}}$ increases for C_p fixed at threshold. Note that the PDF's shown in (b) and (c) may not have unit area, because they do not include portions of $\rho_{\bar{r}}$ that fall below threshold; that case would be represented by a discrete probability category at $P_r = 0$, but inclusion of that category complicates the plots.

the Gabor 50% of the time, but when we do see the Gabor, it can appear to be relatively large because of the steep slope of the $P_r(C_p)$ function.

The final result of the analysis must be that, although contrast threshold decreases with increasing standard deviation of a Gabor, Gaussian standard deviation is not an easily interpretable measure of the influence of cortical (spatial) summation on direction discrimination. Moreover, the noisy nature of perceived size at threshold com-

plicates the picture even further: How does the noise affect the integration process? Our conclusion must be that contrast thresholds with the use of Gaussian-windowed stimuli depend on noisy, contrast-dependent, corticotemporal (spatiotemporal) integration.

6. CONCLUSIONS

Using a simple two-parameter model, we show that our data are very well accounted for by the natural assumption that perceived Gabor size is limited by contrast threshold for the spatial carrier. As predicted by the model, the perceived spatial extent of a Gabor patch varies linearly with the standard deviation of the Gaussian but nonlinearly and monotonically with peak contrast. Moreover, perceived Gabor size for a fixed standard deviation and peak contrast depends nonlinearly and non-monotonically on carrier spatial frequency. At suprathreshold peak contrasts Gabor perceived size is relatively unaffected by systemic noise but varies in a manner that is consistent with the influence of local contrast gain control. However, at and near threshold, noise plays a major role in determining perceived size. We conclude that measures of contrast threshold with the use of Gaussian-windowed stimuli (or any other nonflat contrast window) are determined not just by contrast response of the neurons activated by the stimulus but also by a noisy, contrast-dependent spatiotemporal (corticotemporal) integration volume. Contrast threshold measures with Gaussian-windowed stimuli therefore confound the influence of spatial and temporal integration with observer sensitivity to the drifting carrier.

ACKNOWLEDGMENTS

Eric Fredericksen was supported by the Natural Sciences and Engineering Research Council of Canada through grant OGP0046528. Peter Bex was supported by the Natural Sciences and Engineering Research Council of Canada through grant OGP0001978 and by U.S. Public Health Service grants EY-4885 and EY-1319. Frans Verstraten was supported by a NATO research grant from the Netherlands Organization for Scientific Research (NWO) and a Niels Stensen Foundation postdoctoral award. We thank Fred Kingdom, David Keeble, Stan Klein, and Charles Stromeyer for helpful discussions of these ideas. Finally, we thank two anonymous reviewers for remarks that improved the manuscript.

*Present address, Department of Cognitive Science, SSP-3, University of California, Irvine, Irvine, California 92697; e-mail address, eric@mach2.hipl.uci.edu.

REFERENCES AND NOTES

1. S. J. Anderson and D. C. Burr, "Receptive field size of human motion detection units," *Vis. Res.* **27**, 621-635 (1987).
2. S. J. Anderson and D. C. Burr, "Spatial summation properties of directionally selective mechanisms in human vision," *J. Opt. Soc. Am. A* **8**, 1330-1339 (1991).
3. A. B. Watson and K. Turano, "The optimal motion stimulus," *Vis. Res.* **35**, 325-336 (1995).

4. D. Gabor, "Theory of communication," *J. Inst. Electr. Eng.* **24**, 891–910 (1946).
5. J. G. Daugman, "Spatial visual channels in the Fourier plane," *Vis. Res.* **24**, 891–910 (1984).
6. D. J. Field and D. J. Tolhurst, "The structure and symmetry of simple-cell receptive-field profiles in the cat's visual cortex," *Phys. Rev. B* **228**, 379–400 (1986).
7. R. A. Young, "The Gaussian derivative theory of vision: Analysis of cortical cell receptive field line-weighting profiles," General Motors Research Pub. GMR-4920 (1985).
8. R. A. Young, "The Gaussian derivative model for spatial vision: I. Retinal mechanisms," *Spatial Vision* **2**, 273–293 (1987).
9. Current discussions of this topic can be found with a World Wide Web browser such as Mosaic or Netscape. See the topic "Tutorials, FAQs, and proceedings" at the Universal Resource Locator (URL) designated by <http://vision.arc.nasa.gov/VisionScience/VisionScience.html>.
10. R. B. Tootell, M. S. Silverman, and R. L. De Valois, "Spatial frequency columns in primary visual cortex," *Science* **214**, 813–815 (1981).
11. R. B. Tootell, M. S. Silverman, E. Switkes, and R. L. De Valois, "Deoxyglucose analysis of retinotopic organization in primate striate cortex," *Science* **218**, 902–904 (1982).
12. E. Schwartz, R. B. Tootell, M. S. Silverman, E. Switkes, and R. L. De Valois, "On the mathematical structure of the visuotopic mapping of macaque striate cortex," *Science* **227**, 1065–1066 (1985).
13. C. F. Stromeyer and S. Klein, "Evidence against narrow-band spatial frequency channels in human vision: The detectability of frequency modulated gratings," *Vis. Res.* **15**, 899–910 (1975).
14. We interchangeably refer to this measurement as perceived radius, perceived size, and perceived spatial extent throughout the manuscript.
15. W. H. Press, A. A. Teukolsky, W. T. Vetterling, and B. P. Flannery, *Numerical Recipes in C*, 2nd ed. (Cambridge U. Press, Cambridge, 1992).
16. The contour level is determined as that change in squared error (i.e., error variance) that is different from the minimum error with 95% likelihood. The amount of squared-error change is determined with the standard *F*-ratio test. For details see the handbook for the *Scientist® for Experimental Data Fitting* software package (MicroMath Scientific Software, P.O. Box 71550, Salt Lake City, Utah 84171-0509).
17. For definitions of analysis-of-fit values see the handbook for the *Scientist® for Experimental Data Fitting* software package (MicroMath Scientific Software, P.O. Box 71550, Salt Lake City, Utah 84171-0509).
18. H. Akaike, "A new look at statistical model identification," *IEEE Trans. Autom. Control* **19**, 716–723 (1974).
19. I. Ohzawa, G. Sclar, and R. D. Freeman, "Contrast gain control in the cat's visual system," *J. Neurophysiol.* **54**, 651–667 (1985).
20. D. J. Gelb and H. R. Wilson, "Shifts in perceived size as a function of contrast and temporal modulation," *Vis. Res.* **23**, 71–82 (1983).
21. This situation is made more complicated by the fact that contrast gain control processes occur during the first 500 ms of stimulus presentation [H. R. Wilson and R. Human-ski, "Spatial frequency adaptation and contrast gain control," *Vis. Res.* **33**, 1133–1149 (1993)].
22. A. J. van Doorn and J. J. Koenderink, "Spatiotemporal integration in the detection of coherent motion," *Vis. Res.* **24**, 47–53 (1984).
23. W. A. van de Grind, J. J. Koenderink, and A. J. van Doorn, "The distribution of human motion detector properties in the monocular visual field," *Vis. Res.* **26**, 797–810 (1986).
24. R. E. Fredericksen, F. A. J. Verstraten, and W. A. van de Grind, "Spatial summation and its interaction with the temporal integration mechanism in human motion perception," *Vis. Res.* **34**, 3171–3188 (1994).
25. J. T. Todd and J. F. Norman, "The effects of spatiotemporal integration on maximum displacement thresholds for the detection of coherent motion," *Vis. Res.* **35**, 2287–2302 (1995).
26. R. G. Brown, *Introduction to Random Signal Analysis and Kalman Filtering* (Wiley, New York, 1983), p. 347.
27. A. B. Bonds, "Temporal dynamics of contrast gain in single cells of the cat striate cortex," **6**, 239–255 (1991).
28. M. W. Cannon and S. C. Fullenkamp, "Spatial interactions in apparent contrast: Inhibitory effects among grating patterns of different spatial frequencies, spatial positions and orientations," *Vis. Res.* **31**, 1985–1998 (1991).
29. D. Ariely and C. Burbeck, "Statistical encoding of multiple stimuli: a theory of distributed representation," *Invest. Ophthalmol. Vis. Sci. Suppl.* **36**, 472 (1995).